Ultraintense laser-cluster interactions: Effects of the cluster shape

Kasey Barrington, Zachary Hartwick, Joseph Trost, Rishi Pandit, Nicolas Bigaouette, Lora Ramunno, and Edward Ackad

Phys. Rev. A **93**, 013417 — Published 19 January 2016

DOI: 10.1103/PhysRevA.93.013417

Ultra-Intense Laser-Cluster Interactions: Effects of the Cluster's Shape

Kasey Barrington[1], Zachary Hartwick[1], Joseph Trost[1,3], Rishi Pandit[1]
Nicolas Bigaouette[2], and Lora Ramunno[2], Edward Ackad[1]
[1] *Department of Physics, Southern Illinois University Edwardsville, Edwardsville, IL 62026, USA*
[2] *Department of Physics, University of Ottawa, Ottawa, On K1N 6N5, Canada*
[3] *Department of Physics, University of California, Davis, California 95616, USA*
(Dated: December 30, 2015)

The disintegration of non-icosahedral rare-gas clusters in ultra-intense extreme ultraviolet (XUV) pulses is studied. The clusters quickly form a nanoplasma and evolve only according to the nanoplasma's dynamics which are determined predominately by the cluster's initial shape. It is found that the cluster's disintegration follows a simple model well predicted using only the initial structure. The main finding is that the ions disintegrate tangentially from the surface of the cluster's overall shape. In ellipsoidal clusters, the work done on the ions near the semi-minor axis by the other particles (ions and electrons) is larger than the work done on the ions near the semi-major axis. This leads to an inversion of the ellipsoidal axes due to the different axes expanding at different rates.

I. INTRODUCTION

The extreme ultraviolet regime (XUV), from about 60 -10 nm, represents a unique regime in laser matter interactions of rare-gas clusters [1, 2]. The photon energy is sufficient enough to ionize some of the valence shell electrons, but not the inner shell electrons. Thus, Auger processes do not occur. Further, the ponderomotive energy of electrons in this regime is negligible [3, 4]. Thus, the only communication between the laser pulse and the irradiated matter is by single photon-ionization. This simplifies the analysis and allows for the decoupling of the nanoplasma's inherited dynamics from the laser-driven nanoplasma dynamics.

Rare-gas clusters have been measured [5], and even directly imaged [6], to be icosahedral in shape. However, many other manufactured shapes are possible with other materials, such as: metallic ellipsoidal clusters [5, 7], cylindrical metal or semiconductor cylindrical nanorods [8–10] and spherical metallic clusters [10]. Other, rare-shaped clusters have also been experimentally imaged which are roughly cylindrical [6]. Further, biological macromolecules often take on symmetries that are very close to these simple shapes: virus capsids are almost spherical, GroE chaperonins assist substrate proteins (GroEL:$GroES_2$ complex [11] for instance) are ellipsoidal, and coiled coils and DNA are very much cylindrical.

The ultra-short XUV pulses which are now possible experimentally, permit the exploration of these nanoplasmas [12]. Other work has shown that the disintegration of rare-gas clusters in XUV pulses is a mixture of a Coulomb explosion in the outer shell and a hydrodynamic expansion of the core [1, 13–16]. Further, work has shown that it is the outer shells of the cluster which retain the detected high-charged states [17–20]. The inner ions reach the highest charge state during the life of the nanoplasma [21, 22], but recombine with electrons upon disintegration to yield low charged states in the time-of-flight detector [23]. This work builds on these results to determine the effect of the initial shape of the object on the disintegration products.

In this paper, we model the effect of the initial shape of the cluster on its disintegration dynamics. We do this by considering various rare-gas cluster shapes. Since the laser quickly photo-ionizes any nanomaterial, it is a reasonable approximation to model a wide range of atoms and molecules in these various structures in a similar manner as for rare-gas clusters; the structure merely provides the initial positions of the atoms [24, 25]. However, different materials will have different ionization potentials for their valence electrons. This could be easily taken into account for a specific system, though here we use rare gas ionization potentials as we are focusing our investigation on the role of the target shape. Most of the nanomaterials or biological objects mentioned as prototypes for each shape are roughly homogeneous as the mass difference between many of the constituents is small (in biological molecules, the largest difference is between carbon and oxygen atoms which have a mass difference on the order of the isotope mass difference within each element), except for hydrogen which is largely uniformly distributed throughout the sample. Thus, the dominant approximation for extending this working to biological samples is that the details of the material are quickly lost as the structure becomes a nanoplasma with the shape of the initial structure dominated by the nanoplasma's internal dynamics [26].

The paper is organized as follows. The method used is first explained, followed by the results of spherical clusters. A model is presented for the direction and relative size of the average force felt by each ion as a function of its initial position. Subsequently, an ellipsoidal cluster with the same volume as the spherical cluster is examined. The average force on each ion is again examined and the effects of the initial non-spherical shape on the disintegration are explored. Finally the discussion section summarizes the findings and suggests possible applications of these results.

II. METHODS

The laser-cluster interaction was modeled using a hybrid quantum/classical approach [27] which has been successful in reproducing the results of other rare-gas cluster experiments in the XUV regime [4, 19]. The motion of the ions and electrons is evaluated by molecular dynamics using a velocity verlet algorithm implemented using openCL and run on gpgpus.

Three types of ionization mechanisms are included: single photon-ionization, direct collisional ionization and augmented collisional ionization (ACI). The mechanism of ACI allows for the excitation of a valence electron to a higher electronic state by a collisional electron. The excited valence electron then has a lower ionization potential and different cross-section for a subsequent collisional electron to ionize it (see reference [27] for more details on ACI). Eight of the lowest electronic excited states were included in this work. The ionization is evaluated by cross-sections (both calculated via quantum mechanics codes or taken from experimental data if available). Further, many-body recombination is also included as detailed in reference [4].

As we will show, the results are not sensitive to an atom's exact initial position, but rather to the overall symmetry of the cluster. Thus, for simplicity, we consider an fcc lattice, where the border is cut out into the desired shape.

The simulations begin with the neutral atoms at rest in the initial configuration (fcc forming a sphere or ellipsoid). Each atom is tested for ionization based on the increasing laser intensity (modeled as having a $\sin^4(\omega t)$ intensity envelope) and the atomic cross-sections with the cluster environment accounted for [28, 29]. When ionization does occur the charge state of the atom or ion is incremented and a new electron is added to system with the correct energy relative to the outer-ionization threshold even if it is inner-ionized, as most electrons will be. The force on each particle due to each other (charged) particle is calculated every time step and the particles are moved accordingly (using a velocity verlet algorithm). Further, electrons near (< 4 bohr) a target atom or ion will be tested to see if it can collisionally excite, ionize or recombine with the target. The simulation is brought to an end once the cluster is completely disintegrated (determined when the ion-ion interaction is less than the force caused by a typical time-of-flight electric field of about 400 V/cm). For the current set of parameters, 1 picosecond was found to be sufficient for the smaller sized clusters and 3 picoseconds for the larger clusters.

III. RESULTS

In this section we report on several differently shaped argon-clusters irradiated by a 10 fs laser pulse at 13.7 nm, which is above the inner-shell ionization energy of argon. An intensity of 5×10^{15} W/cm^2 was used to ensure the nanoplasma is created very rapidly and is within experimental accessibility of current free-electron laser facilities. The structures were propagated through a complete disintegration of the structure, determined when the ion-ion interaction was less than a typical time-of-flight field (400 V/cm). A constant time step of 2 attoseconds was used to ensure minimal numerical heating, tested by ensuring the results were well converged for the time-step size. Multiple, independent runs (10 for the sphere and smaller ellipses and 4 for the larger ellipses) were used in sufficient number to give convergent results for all measurements. All data presented is averaged over all the runs with identical initial conditions.

In this regime, only the initial placement of the atoms can have an influence on the disintegration dynamics of the structure. The influence of (possible) molecular bonds is negligible [26] and, thus, not directly modeled.

The laser-field does not contribute to the electron motion in the parameter regimes we consider. The electron's ponderomotive potential is roughly equal to the cluster-bound (inner ionized) electron temperature [30, 31],

$$K_B T = mc^2 \left(\sqrt{1 + \frac{I\lambda^2}{1.37 \times 10^{18}}} - 1 \right) = 0.1 \ eV \quad (1)$$

where K_B is the Boltzmann constant, m is the mass of electron, c is the velocity of light, T is defined as the hot electron temperature, I is the cycle averaged laser intensity in W/cm^2 and λ is the wavelength of the laser in microns. The estimated pondermotive potential energy is 0.1 eV, which is negligible compared with the electron plasma temperature (which is solely caused by single photon-ionization) of about 30 eV. Therefore, the only influence the laser pulse has on the dynamics is through direct photo-ionization during the pulse. After the pulse, the nanoplasma will evolve independently of any outside influences. We construct a toy-model, based solely on the structure's shape, to explain our findings.

A. Spherical Clusters

Spherical clusters represent the simplest symmetry since the disintegration is expected to be radial. Previous work on clusters (icosahedral structures) has shown that the outer-shells explode with the highest charge and kinetic energy [4, 12, 18, 19, 32, 33]. The electrons, upon photo-ionization, are ejected along the electric field axis of the laser. The net momentum transfer is nearly zero since electrons come out in both directions and, thus, the cluster evolves according to the dynamics of the nanoplasma.

The time evolution of the ion-charge distribution (shown in figure 1) for a spherical (fcc-lattice) cluster $N = 530$ measuring about 60 Bohr (32 Å) in diameter clearly displays regular peaks in the radial coordinate, indicating that the ions disintegrate in roughly spherical

shells. These shells are due to the fcc-initial positions still having some radial-periodicity. Any other type of symmetry in the disintegration (including no symmetry at all) would not give clearly defined peaks in the radial coordinate. Thus, the regular peaks are due to the initial structure having some radial periodicity and the disintegration retaining that symmetry.

The last peak is clearly traveling at the highest radial velocity. There is also a clear spread in the width of the radial shells as the cluster disintegrates. The time-cuts at 150, 300, and 450 femtoseconds (shown in the insert of figure 1) show that the initial radial-periodicities remain intact, although they do increase their radial width. The distance between the outermost peak and the next charge peak becomes increasingly large, owing to the fact that the outershell has the most kinetic energy.

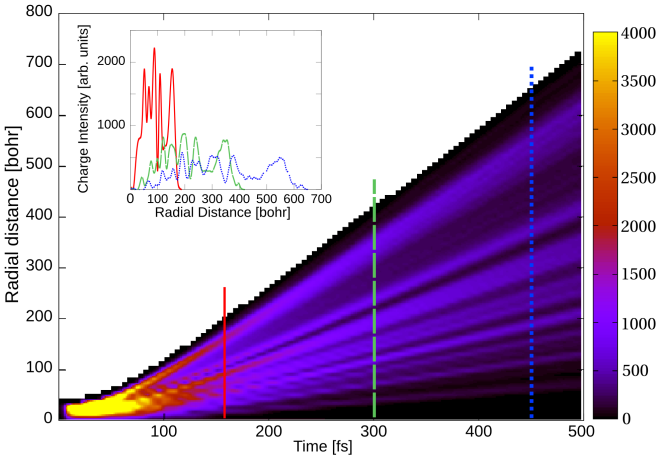

FIG. 1. (Color Online) The total ion-charge distribution as a function of the radial distance from the center of the spherical argon clusters, $N = 530$, irradiated by a 10 fs pulse ($\lambda = 13.7$ nm, $I = 5\times10^{15}$ W/cm^2) as a function of time. The inset corresponds to three time cross-sections corresponding to the vertical lines in the main figure at: 150, 300, and 450 femtoseconds.

A uniform charge density has a well known characteristic shape which is not flat due to the volume of the spherical shell increasing as the radial distance increases. For a fixed shell thickness $\Delta\vec{r}$, the outermost spherical shell will contain a larger volume than an inner spherical-shell. The charge distribution must change by the same amount (as a function of the radial distance) in order to keep the charge density constant. For spherical shells, in order to have a constant density $\rho = C/V$, where ρ is the charge density, C is the total charge and V is the volume of the spherical shell (the ith shell is given by $V_i = \frac{4}{3}\pi\left(r_{i+1}^3 - r_i^3\right)$) the charge, C, must have a radial distribution

$$C \propto r(r - \Delta r) \tag{2}$$

where Δr is the (constant) radial bin width. This is very close to the shape seen in the data for the electron charge distribution (figure 2), supporting the premise of

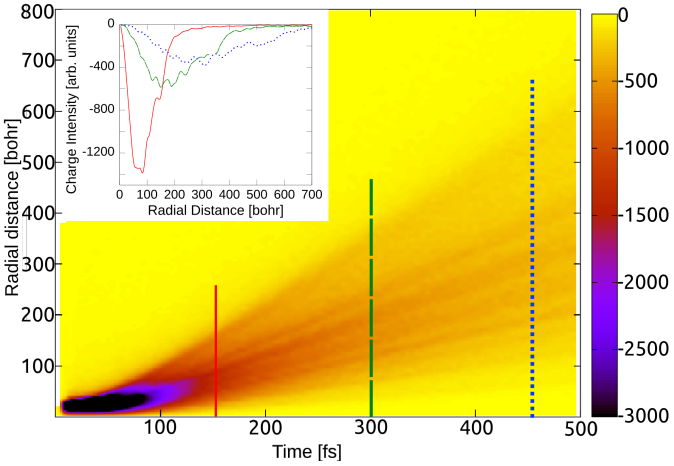

FIG. 2. (Color Online) The total electron-charge distribution as a function of the radial distance from the center of the spherical argon clusters, $N = 530$, irradiated by a 10 fs pulse ($\lambda = 13.7$ nm, $I = 5\times10^{15}$ W/cm^2) as a function of time. The inset is three time cross-sections corresponding to the vertical lines in the main figure at: 150, 300, and 450 femtoseconds.

an almost uniform electron-charge distribution throughout the cluster. They (mostly) do not concentrate around the ion shells. The time cross-sections (figure 2 inset) also show almost smooth distributions throughout the cluster with the characteristic shape of a uniform radial charge distribution.

The total charge distribution of the cluster (figure 3) shows that the core of the cluster is not neutral and is clearly stratified into charged shells. These become increasingly separated. However, the electrons fill the gap between the ion shells essentially uniformly, as observed in figure 2. Interestingly, there is a thick (about 50 Bohr ≈ 26 Å) outside layer of electrons on the surface of the cluster for the first 150 femtoseconds. These are inner-ionized electrons (bound to the cluster) and are a function of the electron-cloud temperature [29]. Outer-ionized and cluster-evaporated thermal electrons do not give a peak since they are unevenly distributed in time (outer-ionized electrons occur only at the very start of the pulse and cluster-evaporated thermal electrons occur spontaneously at any subsequent time).

The cluster's total charge as a function of the radial distance (shown in figure 3) indicates, as expected, that the net charge of the inner-core of the cluster is slightly positive. However, it is clear that the bulk of the charge of the cluster is concentrated on the outershell of the cluster. Further, the bulk of the electrons are outside the cluster (evidenced by the fact that charge is conserved in the calculations so the total charge goes to zero as $r \to \infty$).

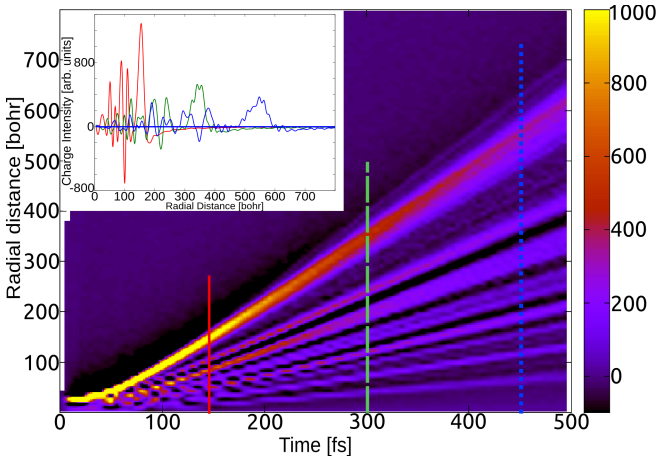

FIG. 3. (Color Online) The total-charge distribution as a function of the radial distance from the center of the spherical argon clusters, $N = 530$, irradiated by a 10 fs pulse ($\lambda = 13.7$ nm, $I = 5 \times 10^{15}$ W/cm^2) as a function of time. The inset are three time cross-sections corresponding to the vertical lines in the main figure at: 150, 300, and 450 femtoseconds.

1. *Disintegration Direction*

Having looked at the particulars of the aforementioned spherical clusters, the goal is now to model the general behavior of the cluster's disintegration in order to obtain general models beyond the currently investigated situations. Towards this end, the direction of the average force that each ion experiences upon disintegration is examined. The direction of the force, for a spherical cluster is, as expected, largely spherical since in the XUV-regime the laser-field only dictates the photo-electron's ionization axis, the laser does not drive the electron's subsequent motion (as is well known in the infrared regime) [34].

We consider a toy-model, where over the course of the cluster's disintegration each ion will feel a radially directed average-force. The direction of the average force (calculated using the full cluster dynamics) is compared with this toy-model.

Using the initial (which is always $\vec{v}$=0) and final (at $t = 1$ ps) velocity of each ion, the actual direction of the average force for each ion is obtained ($\vec{F}_{av} \propto \Delta\vec{v}$, since $\Delta t = 1$ ps will be the same for each ion). To determine how closely the disintegration follows the spherical symmetry of the cluster, the angular deviation from the radial direction is calculated by

$$\theta_{\rm dis} = \cos^{-1}\left(\frac{\vec{v}\cdot\hat{r}}{|\vec{v}|}\right) \tag{3}$$

where $\hat{r}$ is the radial unit vector to the initial position of the ion, and $\vec{v}$ is the final velocity of the ion. The average difference between the calculation and the model (equation 3) over the whole cluster is 2.9 ± 2.0 degrees (where the uncertainty comes from using many ions from distinct runs and having 530 atoms per run) [35]. Thus, the average force on each ion points in the radial direction with only a few degrees of deviation (on average). Taken together with the clear radial peaks of the ions (figure 1), it is clear that *when a spherical cluster disintegrates, it retains its spherical symmetry.*

2. *Average Force*

While the direction of the disintegration may be predicted by the initial symmetry of the spherical cluster, the average force on the ions (and thus their change in momentum) may also be predicted, to a large degree, using the following toy-model.

An ion in the cluster can be modeled as a charge in a homogeneously charged sphere in order to compare the average force on the ion as a function of its initial position. The goal is to determine the magnitude of the average force (throughout the disintegration) an ion will feel based solely on its initial position. The force an ion of charge q would experience is assuming the charge density, ρ, is constant is

$$\vec{F}_{av} = \frac{4\pi k q \rho}{3} r\hat{r}. \tag{4}$$

Thus, the average force experienced by an ion over the course of the entire disintegration is expected to be linear in its *initial* radial position with the assumptions that: *i*) the cluster is uniformly charged, *ii*) the shape of the cluster remains unchanged during the disintegration and, *iii*) the interaction time (in the case of the impulse) and/or distance (in the case of the work) is the same for all ions. For the complete spherical cluster the average percent difference between the toy-model (equation 4) and the full calculations is 14.3 ± 2.0 %, where the uncertainty stems from using multiple runs and all the ions in the cluster [35]. The dominant source of error is from the ions in the core of the cluster. The outer shells, however, follow the model quite well. A percent error just under 9.8 ± 2.7 % is obtained when only the outermost shell is used (atoms within 4 Å of the outer surface of the cluster). Thus, the magnitude of the average force an ion will experience throughout the cluster's disintegration is given by equation 4 (to within better than 15%) which is only a function of the ion's initial position.

The agreement between the toy-model and the full calculation allow for the following conclusion: *The spherical cluster disintegrates radially with a homogeneous charge throughout the cluster.*

B. Ellipsoidal Clusters

To extend the model beyond spherical shapes, we now present results for ellipsoidal clusters. Ellipsoidal clusters represent a departure from spherical clusters in one

or two dimensions. In reducing the symmetry of the cluster, it is demonstrated that while simple principles are at work the consequences of these are non-intuitive.

An ellipsoidal surface is defined by

$$S(x,y,z) = \left(\frac{x}{a}\right)^2 + \left(\frac{y}{b}\right)^2 + \left(\frac{z}{c}\right)^2 - \mu = 0, \qquad (5)$$

where μ is the average radius of the ellipsoid, or the radial-like coordinate in ellipsoidal coordinates. Different μ values define ellipsoidal surfaces (homeoids). These will be used to subdivide the ellipsoidal cluster into (ellipsoidal) shells of constant μ (as was done using the radial coordinate for spherical clusters).

A parameterization of the degree to which an ellipsoid is non-spherical, but retains the same volume is needed. To accomplish this, one axis is fixed to the radius of a spherical cluster, a. The other two axes are then adjusted to keep the volume the same as a spherical cluster of radius a. We introduce the sphericity parameter

$$s = \frac{b}{a} = \frac{a}{c} \qquad (6)$$

as a measure of the sphericity of the ellipsoid where the larger the number the more spherical, with $s = 1$ being a perfect sphere. The parameter c is the semi-major axis while the parameter b is the semi-minor axis, leaving a to be $b < a < c$. This is commonly referred to as a tri-axial ellipsoid.

A 490 atom ellipsoidal cluster with the same volume as the spherical cluster in section III A with a spheroidicity of $s = 0.7$ (mostly spherical) is examined first ($a = 15.7$ Å, $b = 10.5$ Å, $c = 20.9$ Å).

The ellipsoidal cluster does not expand spherically, unlike the spherical cluster. Nor does the ellipsoidal cluster expand in ellipsoidal shells (as shown in figure 4), since an ellipsoidal expansion would have strong, consistent, striations as was seen for the spherical cluster in figure 1. In fact, the ellipsoidal cluster *inverts* along *each* axis. The full width at half the maximum (FWHM) of the semi-major axis (z-axis) expands at the slowest rate while the FWHM of the semi-minor axis (y-axis) expands at the fastest rate. Examining the ion distribution of the cluster along each Cartesian axis (figure 5) it is clear that the cluster, while still expanding in all directions (note the different horizontal ranges in figure 5), expands along the semi-minor axis most rapidly. This leads to an inversion of the ion distribution (depicted in figure 5).

The initial shape of the cluster is that of a tri-axial ellipsoid ($c > a > b$ as shown in the top plot of figure 5). Upon ionization, the ions closest to the center of the cluster, radially (demonstrated in section III B 2), experience the largest average force. The ions furthest from the center of the cluster experience a comparatively smaller average force. Thus, the ions closest to the center of the ellipsoid, along the semi-minor axis, accelerate away from the cluster more rapidly than the ions along the other two axes. The other axes' ions are also accelerating away from the cluster, but more slowly. At

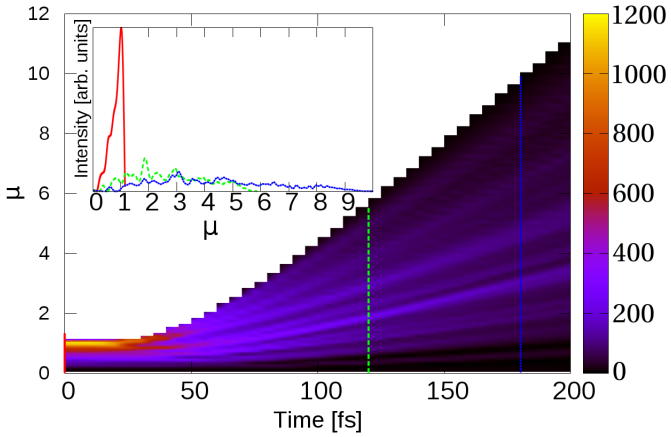

FIG. 4. (Color Online) The ion distribution as a function of time and the ellipsoidal coordinate μ (which defines concentric homoeiods) for an ellipsoidal argon cluster, $N = 490$ and $s = 0.7$ (with the same volume as the $N = 530$ spherical clusters), irradiated by a 10 fs pulse ($\lambda = 13.7$ nm, $I = 5 \times 10^{15}$ W/cm^2). The initial outer edge of the ellipse defines $\mu = 1$.

around 120 fs the cluster now has a roughly spherical shape, with all sides around the same size (middle plot in figure 5 where the size of the cluster is defined as the FWHM of the ion distribution). Note that the cluster is still expanding resulting in a different scale for horizontal axis in each plot. Finally, at around 180 fs, the size ordering of each axis has been fully reversed. The initial semi-minor axis, y, is now the semi-major axis, while the initially semi-major axis, z, is now the semi-minor axis. Thus, during the disintegration the ellipsoidal cluster has inverted its shape.

The ion-charge distribution was also investigated and is shown in figure 6. The first thing of note is that the highest charge density scale is five times larger than that of the ion-number distribution (figure 4), indicating that the average charge state along the outer ellipsoidal shell (where the peak is) has an average charge state of 5. Another result of note is that the ion-charge distribution is clearly proportional to the ion-number distribution (figure 4) after about 25 fs (once the cluster has become significantly charged). This proportionality indicates that at this high intensity, in small clusters, the charge-states are roughly uniformly distributed. The outermost ions experience the largest force and thus the initial high-charge striation splits, as in the ion-number distribution (figure 4). These outermost ions remain the furthest and retain the asymmetry of the initial structure (as may also be viewed in figure 5 where the tails of the distribution) retain the original ordering. To be clear, the inversion seen in these ellipsoidal clusters is an inversion of the FWHM, not the outershell which retains its original shape (while expanding).

Since electrons move much more rapidly than the ions, and at the start there are not many of them, the electron spatial distribution was calculated differently. The peak

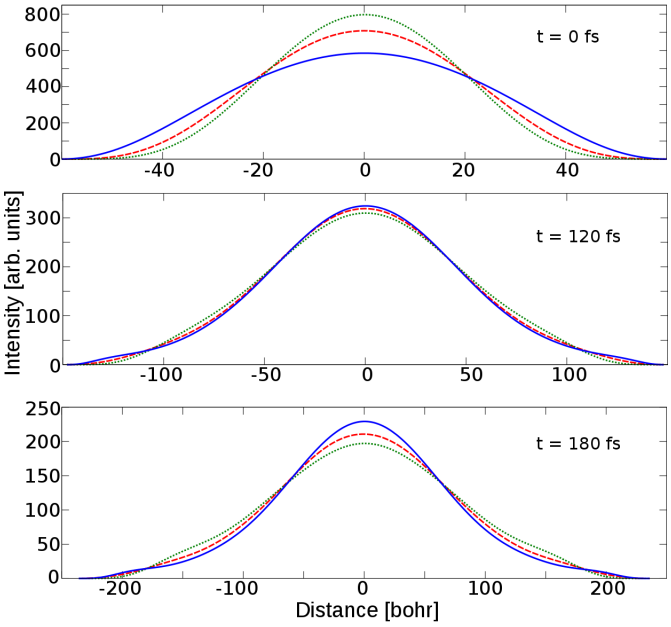

FIG. 5. (Color Online) The ion distribution along each Cartesian axis at three different times for an ellipsoidal cluster, $N = 490$ and $s = 0.7$ (with the same volume as the $N = 530$ spherical clusters), irradiated by a 10 fs pulse ($\lambda = 13.7$ nm, $I = 5 \times 10^{15}$ W/cm^2). Initially the semi-major axis is the (blue) solid line, but due to the inversion (see text) the (green) dashed line ends up being the semi-major axis. Note the change in the distance scale for each plot.

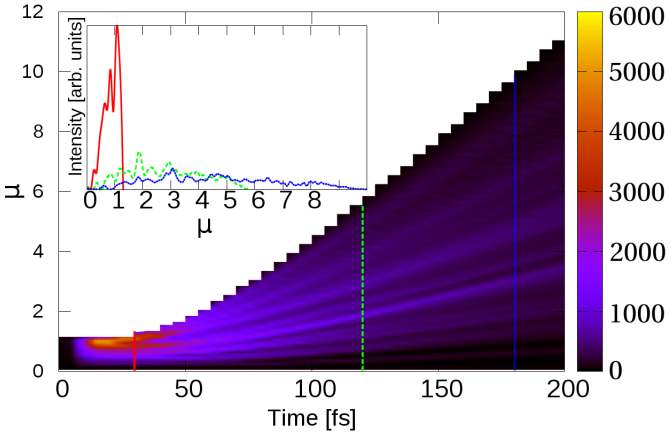

FIG. 6. (Color Online) The ion-charge distribution as a function of time and the ellipsoidal coordinate μ (which defines concentric homoeiods) for an ellipsoidal argon cluster, $N = 490$ and $s = 0.7$ (with the same volume as the $N = 530$ spherical clusters), irradiated by a 10 fs pulse ($\lambda = 13.7$ nm, $I = 5 \times 10^{15}$ W/cm^2). The initial outer edge of the ellipse defines $\mu = 1$.

of the electron distribution was found (maximum). Then the FWHM was determined directly from the full electron distribution (without assuming a type of distribution).

The electron distribution's FWHM (not shown) begins as being roughly prolate ($a \approx b < c$) and becomes inverted, with the same ordering as the ion-distribution ($b > a > c$). *Thus, the electron spatial distribution follows the same spatial distribution as the ions.*

The total charge distribution of the ellipsoidal cluster has a core that is, overall, positively charged, while the exterior of the cluster remains largely negatively charged (shown in figure 7). A halo of electrons remain bound to the charged core, equal in all directions. This is similar to the electron halo found in the spherical cluster (see the large, black striation in figure 3). The timescale of the transition from tri-axial to roughly spherical matches that of the ion-number distribution which indicates that the electrons follow the same transition (otherwise the total charge distribution would differ, at the same time, form the ion-number distribution).

The total charge distribution is initially asymmetric, following the ion distribution, but quickly becomes symmetric (shown in figure 7). This is expected since the electrons move rapidly toward the regions of highest charge, eventually screening all the ion charges equally. After 120 fs, the total charge is symmetric despite the asymmetry in the ion distribution. Thus, the electron distribution, as previously stated, follows that of the ions.

The nanoplasma is, thus, tri-axial and in the opposite ordering from the initial ion setup (initially $c > a > b$, subsequently $b > a > c$).

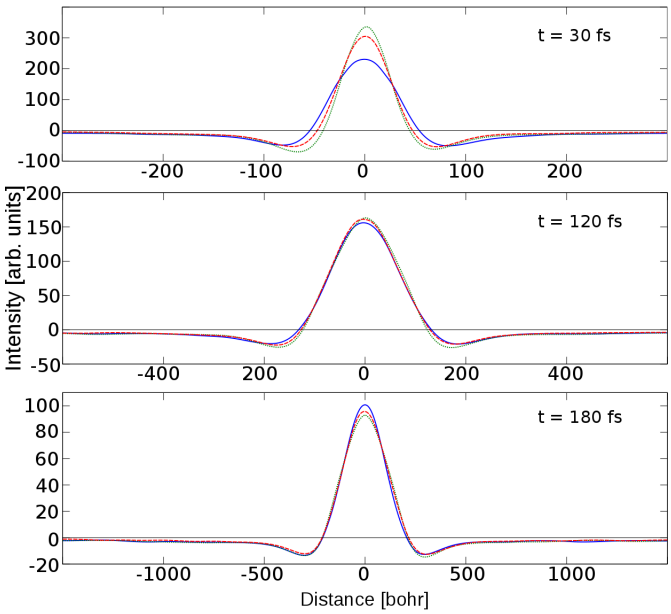

FIG. 7. (Color Online) The total-charge distribution along each Cartesian direction with the same (colors and) linestyles as figure 5, at different times. Note the different distance ranges in each plot.

1. Disintegration Direction

As in the case of the spherical cluster (c.f. section III A 1), a model for the generic behavior of the ions in the cluster upon disintegration is sought. Modeling the ellipsoidal cluster as a charged conductor, it is expected that the direction of the average force will be normal to the surface of the cluster. Thus, the direction of the average force is modeled as

$$\hat{F}_{av} = \hat{n} = \frac{\nabla S}{|\nabla S|}, \tag{7}$$

where S is the definition of the ellipsoidal cluster in equation 5. The predicted direction of the average force (normal to the surface) is then normal to the atom's initial homeoid and is given by $\hat{n}$.

To assess how well this toy-model matches with the full calculations, we again examine the angular deviation between the full calculation and the toy-model. The angular deviation from the (predicted) normal direction is given by

$$\theta_{\text{dis}} = \cos^{-1}\left(\frac{\vec{v}\cdot\hat{n}}{|\vec{v}|}\right) \tag{8}$$

where $\hat{n}$ is the normal vector of the initial position of the ion, and $\vec{v}$ is the final velocity of the ion. The average difference between the calculation and the model (equation 8) over the whole cluster is under 7.5 ± 3.5 degrees [35]. Using only the outer homeoid shell the angular deviation is about 6.5 ± 2.8 degrees. Thus, in ellipsoidal clusters, each ion will disintegrate in a direction tangential (to within better than 8 degrees) to the surface of its homeoid.

2. Average Force

The magnitude of the average force is now examined to illuminate how the shape of the cluster inverts. Initially ellipsoidal models were examined under the assumption that the magnitude of the average force an ion would experience would be proportional to the ion's initial ellipsoidal-radial distance (μ). These models failed to match the calculated average force (errors > 50 %). In retrospect, this is not surprising as an ellipsoidal model would require the ellipsoidal cluster to retain its shape upon disintegration, which it does not (aside from the outermost homeoid).

A spherical model, identical to the one in section III A 2, was used instead. This spherical toy-model resulted in a percent difference of 27.8 ± 9.1 % [35]. When only the outer homeoid is considered (atoms within 4 Å of the outer surface of the cluster) the percentage difference drops to 18.1 ± 4.2 %. Despite the complicated dynamics, non uniformity of the spatial charge distribution, a simple picture of the disintegration of an ellipsoidal cluster emerges: *the ions disintegrate in a direction normal to the surface of the structure with an average force that is proportional to the ions original radial distance* (from the cluster's center).

The inversion of the cluster's semi-minor and semi-major axis is understood by the average force model in conjunction with the *increased* interaction time/distance along the semi-minor axis compared with the semi-major axis. This violates the *iii* assumption in section III A 2, and thus, the model becomes increasingly inaccurate as more inner homeoids are included. Ions at the tip of the semi-major axis of the cluster experience the largest average force in the aforementioned spherical model (since the force is $\propto r$). However, the work done on those ions by the other particles is less (acting over a shorter distance and for a shorter time). The final position of the ions ($\Delta\vec{r}$) is dependent on the interaction time as well as the force ($\Delta\vec{r} \propto \vec{F}t^2$). Thus, the inversion occurs because the ions closest to the semi-minor axis have more work done on them (by the other particles) and reach higher velocities. This allows the ions near semi-minor axis to overtake (in terms of radial distance) the semi-major axis ions, inverting the structure's shape.

C. Other Ellipsoidal Clusters

Next, a less spherical cluster ($s = 0.5$) with the same volume is examined to further assess the predictive power of the toy-models. The cluster contains 485 atoms (a = 15.7 Å, b = 7.8 Å, c = 31.4 Å).

While the semi-major axis is now quadruple the width of the semi-minor axis, the inversion still takes place at (around) the same time: all sides being equal occurring at around 120 fs (similar to figure 5) as well as the inversion being completed by 180 fs.

Extending the analysis to larger clusters all of the findings remain consistent. The inversion for larger clusters occurs in a shorter time (around 60 fs for all sides to be equal and 120 fs for the inversion to be complete) for both spheroidicity parameters; $s = 0.7$ ($N = 2183$, a = 26.2 Å , b = 18.3 Å, c = 36.62 Å), and $s = 0.5$ ($N = 2167$, a = 26.2 Å, b = 13.1 Å, c = 52.3 Å).

Further, the disintegration direction of all the aforementioned clusters continues to agree well with the toy-model in equation 7. The quantitative results are summarized in table I.

The angular deviation is significantly closer to zero degrees for clusters which are more spherical ($s = 0.7$). However, much of this is attributed to the construction of an ellipsoidal cluster from an fcc lattice as determined by the location of the ions with the largest deviations [35]. The outer homeoid is only marginally better than the calculation for the total cluster (all ions except the middle ion located at the origin) in all cases. *Thus, the direction of the ion's disintegration is well predicted by its initial position.*

Cluster Size	spheroidicity (s)	Outer homeoid Angular Deviation (degrees)	Total Angular deviation (degrees)	Outer homeoid $\|F_{av}\|$ (percent difference)	Total $\|F_{av}\|$ (percent difference)
490	0.7	6.5 ± 2.8	7.5 ± 3.5	18.1 ± 4.2	27.8 ± 9.1
2183	0.7	6.4 ± 4.4	6.8 ± 4.6	13.1 ± 4.7	25.1 ± 9.8
485	0.5	12.6 ± 5.4	13.6 ± 7.2	22.7 ± 8.4	33.0 ± 9.5
2167	0.5	10.3 ± 5.4	12.0 ± 7.2	26.9 ± 9.0	39.8 ± 16.0

TABLE I. A comparison of all the ellipsoidal clusters with the angular disintegration and average force models for the whole cluster (labeled total) as well as the results for only the outermost homeoid (labeled Outer homeoid). Angular deviations are calculated using equation 8.

The average force model, as expected and explained in section III B 2, is quite accurate for the outermost homeoid compared with the toy-model for all the homeoids (called Total $|F_{av}|$ in table I), but it is consistently better for the more spherical clusters. This is consistent with its formulation while still providing a toy-model to understand the complicated disintegration of a non-spherical structure in simple terms.

The causes of the inversion remain the same: the ions near the semi-minor axis have more work done on them (by the other particles) than the ions along the semi-major axis in the direction which is tangential to their initial position.

IV. CONCLUSION

As more structures are exposed to ultra-intense X-ray laser pulses at free-electron facilities, an understanding of the disintegration dynamics becomes increasingly useful. It is possible to roughly predict the disintegration dynamics knowing only the overall shape of a biological sample or nanostructure. All structures have their ions predominately disintegrate in a direction tangential to the overall shape of the structure. In fact, even more complicated structures, such as the double stranded helix of DNA, has been shown to follow this pattern [36].

Such knowledge may find uses at free-electron laser facilities attempting to image biological samples. Using multiple, orthogonal ion detectors some orientation information about the target can be obtained. For example a long, cylindrical, protein (such as DNA or a coiled coil) would create a large ion signal in the detector perpendicular to its length and a small ion signal in a detector parallel to its length. This could be used to sort vertically-aligned targets from unaligned targets, for example, decreasing the data and time needed to solve the target's structure.

In the case of biological samples, crystal structures must be obtained when the sample is solvated (in order to be useful). However, solvating the sample results in a spherical drop with the sample's shape completely obscured by the water (every sample would be a sphere). Further complicating matters is the fact that the oxygen in water cannot be distinguished from the oxygen in the sample. These issues may be overcome by only allowing a few layers of water to surround the sample (perhaps using nanochannels) in which case the overall shape of the sample is preserved. Another possible method is by immediately freezing (and then possibly tapering the sample [37]) with ultra-cold gases and imaging the sample almost immediately after the sample is frozen (to avoid large scale motions away from the solvated structure) [38].

Non-spherical structures expand at different rates along different axis. The widest axis becomes the largest and vice versa (in terms of the FWHM, the outermost shell retains the original symmetry). Such asymmetry could be exploited, for instance, to allow for a cluster to have multiple instances (along different axes) in which the structure's nanoplasma is at the Mie plasmon resonance [1, 39].

In summary, non-spherical nanostructures exposed to ultra-intense X-ray laser pulses disintegrate in a pattern which is perpendicular to their overall shape. The relative average force on each particle is somewhat predictable. The relative magnitude of the average force on each ion is well modeled and explains how non-spherical structures expand most rapidly along their smallest dimension and vice versa.

V. ACKNOWLEDGEMENTS

This material is based upon work supported by the Air Force Office of Scientific Research under AFOSR Award No FA9550-14-1-0247, SIUE's Research Equipment & Tools grant and SIUE's Seed Grants for Transitional and Exploratory Projects. E. Ackad would like to thank D. Kaplan and M. S. Yousef for useful discussions.

[1] U Saalmann, Ch Siedschlag, and J M Rost. Mechanisms of cluster ionization in strong laser pulses. *Journal of Physics B: Atomic, Molecular and Optical Physics*, 39(4), February 2006.

[2] Th. Fennel, K.-H. Meiwes-Broer, J. Tiggesbäumker, P. M. Dinh, and E. Suraud. Laser-driven nonlinear clus-

ter dynamics. *Reviews of Modern Physics*, 82(2):1793–1842, June 2010.

[3] Christoph Bostedt, Heiko Thomas, Matthias Hoener, Thomas Möller, Ulf Saalmann, Ionuţ Georgescu, Christian Gnodtke, and Jan-Michael Rost. Fast electrons from multi-electron dynamics in xenon clusters induced by inner-shell ionization. *New Journal of Physics*, 12(8):083004, 2010.

[4] Edward Ackad, Nicolas Bigaouette, Stephanie Mack, Konstatin Popov, and Lora Ramunno. Recombination effects in soft-x-ray cluster interactions at the xenon giant resonance. *New Journal of Physics*, 15(5):053047, 2013.

[5] J. C. Phillips. Chemical bonding, kinetics and the approach to equilibrium structures of simple metallic, molecular, and network microclusters. *Chemical Reviews*, 86(3):619–634, 1986.

[6] C. Bostedt, E. Eremina, D. Rupp, M. Adolph, H. Thomas, M. Hoener, A. de Castro, J. Tiggesbäumker, K.-H. Meiwes-Broer, T. Laarmann, H. Wabnitz, E. Plönjes, R. Treusch, J. Schneider, and T. Möller. Ultrafast X-Ray Scattering of Xenon Nanoparticles: Imaging Transient States of Matter. *Physical Review Letters*, 108(9):1–5, February 2012.

[7] Keith Clemenger. Ellipsoidal shell structure in free-electron metal clusters. *Physical Review B*, 32(2):1359–1362, July 1985.

[8] Babak Nikoobakht and Mostafa A. El-Sayed. Preparation and Growth Mechanism of Gold Nanorods (NRs) Using Seed-Mediated Growth Method. *Chemistry of Materials*, 15(10):1957–1962, May 2003.

[9] J Perezjuste, I Pastorizasantos, L Lizmarzan, and P Mulvvaney. Gold nanorods: Synthesis, characterization and applications. *Coordination Chemistry Reviews*, 249(17-18):1870–1901, September 2005.

[10] Victor F. Puntes, Kannan M. Krishnan, and A. Paul Alivisatos. Colloidal Nanocrystal Shape and Size Control: The Case of Cobalt. *Science*, 291(5511):2115–2117, March 2001.

[11] Xue Fei, Xiang Ye, Nicole A LaRonde, and George H Lorimer. Formation and structures of GroEL:GroES2 chaperonin footballs, the protein-folding functional form. *Proceedings of the National Academy of Sciences of the United States of America*, 111(35):12775–80, September 2014.

[12] H. Thomas, A. Helal, K. Hoffmann, N. Kandadai, J. Keto, J. Andreasson, B. Iwan, M. Seibert, N. Timneanu, J. Hajdu, M. Adolph, T. Gorkhover, D. Rupp, S. Schorb, T. Möller, G. Doumy, L. F. DiMauro, M. Hoener, B. Murphy, N. Berrah, M. Messerschmidt, J. Bozek, C. Bostedt, and T. Ditmire. Explosions of xenon clusters in ultraintense femtosecond x-ray pulses from the lcls free electron laser. *Phys. Rev. Lett.*, 108:133401, Mar 2012.

[13] Md. Islam, Ulf Saalmann, and Jan Rost. Kinetic energy of ions after Coulomb explosion of clusters induced by an intense laser pulse. *Physical Review A*, 73(4):38–41, April 2006.

[14] Christian Gnodtke, Ulf Saalmann, and Jan M. Rost. Ionization and charge migration through strong internal fields in clusters exposed to intense x-ray pulses. *Phys. Rev. A*, 79(4):041201, 2009.

[15] B Ziaja, H Wabnitz, E Weckert, and T Möller. Femtosecond non-equilibrium dynamics of clusters irradiated with short intense vuv pulses. *New Journal of Physics*, 10(4):043003, 2008.

[16] Christian Peltz, Charles Varin, Thomas Brabec, and Thomas Fennel. Time-Resolved X-Ray Imaging of Anisotropic Nanoplasma Expansion. *Physical Review Letters*, 113(13):133401, September 2014.

[17] M Hoener, C Bostedt, H Thomas, L Landt, E Eremina, H Wabnitz, T Laarmann, R Treusch, a R B De Castro, and T Möller. Charge recombination in soft x-ray laser produced nanoplasmas. *Journal of Physics B: Atomic, Molecular and Optical Physics*, 41(18):181001, September 2008.

[18] H Thomas, C Bostedt, M Hoener, E Eremina, H Wabnitz, T Laarmann, E Plönjes, R Treusch, A R B de Castro, and T Möller. Shell explosion and core expansion of xenon clusters irradiated with intense femtosecond soft x-ray pulses. *Journal of Physics B: Atomic, Molecular and Optical Physics*, 42(13):134018, 2009.

[19] Edward Ackad, Nicolas Bigaouette, Kyle Briggs, and Lora Ramunno. Clusters in intense xuv pulses: effects of cluster size on expansion dynamics and ionization. *Phys. Rev. A*, 83:063201, Jun 2011.

[20] K. I. Popov, V. Yu. Bychenkov, W. Rozmus, and L. Ramunno. A detailed study of collisionless explosion of single- and two-ion-species spherical nanoplasmas. *Physics of Plasmas*, 17(8):–, 2010.

[21] L. Schroedter, M. Müller, A. Kickermann, A. Przystawik, S. Toleikis, M. Adolph, L. Flückiger, T. Gorkhover, L. Nösel, M. Krikunova, T. Oelze, Y. Ovcharenko, D. Rupp, M. Sauppe, D. Wolter, S. Schorb, C. Bostedt, T. Möller, and T. Laarmann. Hidden Charge States in Soft-X-Ray Laser-Produced Nanoplasmas Revealed by Fluorescence Spectroscopy. *Physical Review Letters*, 112(18):183401, May 2014.

[22] M Müller, L Schroedter, T Oelze, L Nösel, A Przystawik, A Kickermann, M Adolph, T Gorkhover, L Flückiger, M Krikunova, M Sauppe, Y Ovcharenko, S Schorb, C Bostedt, D Rupp, T Laarmann, and T Möller. Ionization dynamics of XUV excited clusters: the role of inelastic electron collisions. *Journal of Physics B: Atomic, Molecular and Optical Physics*, 48(17):174002, September 2015.

[23] Mathias Arbeiter, Christian Peltz, and Thomas Fennel. Electron-relocalization dynamics in xenon clusters in intense soft-x-ray fields. *Physical Review A*, 89(4):043428, April 2014.

[24] Ulf Saalmann, Alexey Mikaberidze, and Jan M. Rost. Spatial Correlations in Finite Samples Revealed by Coulomb Explosion. *Physical Review Letters*, 110(13):133401, March 2013.

[25] T. Laarmann, A. R. B. de Castro, P. Gürtler, W. Laasch, J. Schulz, H. Wabnitz, and T. Möller. Interaction of argon clusters with intense vuv-laser radiation: The role of electronic structure in the energy-deposition process. *Phys. Rev. Lett.*, 92:143401, Apr 2004.

[26] Richard Neutze, Remco Wouts, David van der Spoel, Edgar Weckert, and Janos Hajdu. Potential for biomolecular imaging with femtosecond x-ray pulses. *Nature*, 406:752–757, 2000.

[27] Edward Ackad, Nicolas Bigaouette, and Lora Ramunno. Augmented collisional ionization via excited states in xuv cluster interaction. *J. Phys. B*, 44:165102, 2011.

[28] Thomas Fennel, Lora Ramunno, and Thomas Brabec. Highly charged ions from laser-cluster interactions:

Local-field-enhanced impact ionization and frustrated electron-ion recombination. *Phys. Rev. Lett.*, 99(23):233401, 2007.

[29] Jeff White and Edward Ackad. A validation of a simple model for the calculation of the ionization energies in x-ray laser-cluster interactions. *Physics of Plasmas (1994-present)*, 22(2):–, 2015.

[30] Rishi R. Pandit and Yasuhiko Sentoku. Higher order terms of radiative damping in extreme intense laser-matter interaction. *Physics of Plasmas*, 19(7):073304, July 2012.

[31] S. C. Wilks, W. L. Kruer, M. Tabak, and A. B. Langdon. Absorption of ultra-intense laser pulses. *Physical Review Letters*, 69(9):1383–1386, August 1992.

[32] B. F. Murphy, K. Hoffmann, A. Belolipetski, J. Keto, and T. Ditmire. Explosion of xenon clusters driven by intense femtosecond pulses of extreme ultraviolet light. *Phys. Rev. Lett.*, 101(20):203401, 2008.

[33] B. Schütte, M. Arbeiter, Th. Fennel, M.?J.?J. Vrakking, and A. Rouzée. Rare-Gas Clusters in Intense Extreme-Ultraviolet Pulses from a High-Order Harmonic Source. *Physical Review Letters*, 112(7):073003, February 2014.

[34] Thomas Brabec, editor. *Strong Field Laser Physics*, volume 134 of *Springer Series in Optical Sciences*. Springer, 2009.

[35] The average deviation from the direction model, for each atom, is shown in the upper figure of the Supplemental Material at [url will be inserted by publisher to sphereN530.png]. The percent difference from the force model, for each atom, is shown in the lower figure in Supplemental Material at [url will be inserted by publisher to sphereN530.png]). The average deviation from the direction model, for each atom, is shown in the upper figure of the Supplemental Material at [url will be inserted by publisher ellipse_err_N490_e0.7.png]. The percent difference from the force model, for each atom, is shown in the lower figure of the Supplemental Material at [url will be inserted by publisher ellipse_err_n490_e0.7.png]. See supplemental material at [url will be inserted by publisher to ellispe_07_N490sm.avi] which animates the outer shell of the $s = 0.7$ $N = 490$ ellipsoidal cluster and shows the angular deviation as a function of the initial position, indicated by the color of the ion with blue being the smallest angular deviation and red being the largest.

[36] Joseph Trost, Edward Ackad, Nicolas Bigaouette, and Lora Ramunno. Explosion of non-spherical clusters due to irradiation with intense femtosecond x-rays. In *Frontiers in Optics Conference*, page FW5G.5. Optical Society of America, 2012.

[37] B. Ziaja, H. N. Chapman, R. Santra, T. Laarmann, E. Weckert, C. Bostedt, and T. Möller. Heterogeneous clusters as a model system for the study of ionization dynamics within tampered samples. *Physical Review A*, 84(3):033201, September 2011.

[38] The original idea for flash freezing the sample was given by Enam Chowdhury at the 2015 AFOSR USP program review.

[39] T. Ditmire, T. Donnelly, A. M. Rubenchik, R. W. Falcone, and M. D. Perry. Interaction of intense laser pulses with atomic clusters. *Physical Review A*, 53(5):3379–3402, May 1996.